第 48 卷 第 22 期/2021 年 11 月/中国激光 研究论文

中国激光

2060 铝锂合金光纤激光焦点旋转填丝焊工艺研究

武强*，姜仁杰，李新桐，邹江林，肖荣诗

北京工业大学材料与制造学部智能光子制造研究中心，北京 100124

摘要 采用光纤激光焦点旋转的焊接方法进行 2 mm 厚 2060 铝锂合金薄板填丝(ER4047)焊接试验。利用高速摄像仪观察焊丝熔滴过渡行为及熔池流动行为，采用光学显微镜、能谱仪、X 射线衍射仪、扫描电镜、显微硬度仪及拉伸试验机对焊缝成形质量、气孔形貌、显微组织、化学成分、断口形貌、硬度及接头强度进行分析。结果表明：旋转的激光焦点周期性地作用在熔池及焊丝末端，致使熔池长度增加，熔池流动更平稳且波动幅度减小；焦点旋转可以有效改善焊缝成形，抑制飞溅和气孔的产生；焊缝等轴细晶区的宽度及该区的晶粒尺寸减小，靠近细晶区的柱状晶尺寸也有所减小。与非激光焦点旋转焊接接头相比，激光焦点旋转焊接接头熔合线附近的显微硬度和强度略有升高，接头断裂在熔合线附近，断口呈混合断裂特征。

关键词 激光技术；铝锂合金；填丝焊接；光纤激光；焦点旋转；组织；力学性能

中图分类号 TG442 **文献标志码** A **doi**：10.3788/CJL202148.2202012

1 引 言

2060 铝锂合金作为一种新型的 Al-Cu-Li 系铝合金，具有密度小、比强度和弹性模量高、疲劳性能优异等特点[1]。用铝锂合金取代常规的高强铝合金可使结构重量减轻 10%～15%，刚度提高 15%～20%，因而铝锂成为现代飞机工业中实现结构减重和性能提高的优选材料。光纤激光具有波长短、室温吸收率高、传输柔性好等特点，是实现高效高质量焊接铝锂合金的较为理想的热源[2-3]。但铝合金光纤激光深熔焊接存在焊接过程不稳定、容易产生飞溅和咬边、焊缝成形不良等缺陷[4]。另外，铝锂合金热膨胀系数大、元素易烧损等材料特性使得接头软化、热裂纹倾向大和气孔抑制困难一直以来都是困扰铝锂合金激光焊接应用的主要问题[5]。

相关研究表明：焊前对铝锂合金表面的氧化膜进行机械及化学铣削处理，可以有效减少焊接气孔[6]；将一束离焦激光用于表面重熔，一束聚焦激光用于深熔焊接的双光束焊接方式，在无需进行任何表面预处理的条件下，可以显著减少焊接接头中的氢气孔[6-8]。另外，通过在焊丝中添加稀土元素 Zr、Ce、Sc 等，可以细化焊缝结晶组织，抑制晶界稳定相过量析出，抑制热裂纹，提高焊缝的强度和拉伸性能[9-10]。有人采用 5087 或 4047 填充焊丝对铝锂合金进行了激光焊接，他们发现，通过引入合金元素(如 Li、Cu、Mg 或 Si)可以增加熔池凝固过程中晶界处低熔点共晶的数量，有利于及时愈合凝固过程中可能产生的裂纹，从而降低了液化裂纹的敏感性[11-13]。Twardowska 等[14]发现，焊后热处理(固溶、淬火和时效处理)可以提升 Al-Li-Cu-Mg-Zr 合金焊接接头的抗拉强度和延伸率。

有人发现，激光焦点高频摆动可以有效调控深熔小孔的行为，减少焊接飞溅，提高焊接过程的稳定性[15]。对 AA6061 铝合金进行激光焦点高频摆动焊接时，焦点的高速运动可以打乱 AA6061 铝合金的枝晶结构，细化晶粒，提高焊缝的硬度和塑性[16]。本课题组的前期研究结果表明，采用激光焦点高频旋转的焊接方式可以主动调控母材的熔化/凝固行为，稳定焊接过程，大幅减少纯铝非穿透焊接时的气孔数量和飞溅，改善焊缝的表面质量，提高焊缝的力

收稿日期：2021-05-11；**修回日期**：2021-05-29；**录用日期**：2021-06-15

基金项目：国家自然科学基金面上项目(51775009)

通信作者：*jlwuqiang@bjut.edu.cn

学性能[17]。在此基础上，本课题组采用光纤激光焦点高频旋转的焊接方式，以 4047 焊丝为填充材料，对 2 mm 厚 2060 铝锂合金薄板进行焊接试验，分析了激光焦点旋转对焊缝成形质量、焊接气孔、焊缝微观组织及接头力学性能的影响规律。

2 材料与方法

焊接试验中的基材选用 T8 态 2060 铝锂合金，其规格为 100 mm×60 mm×2 mm。焊丝选用 4047 焊丝，其直径为 1.2 mm。基材表面采用化学铣削方法进行预处理，先采用 NaOH 溶液（溶液中 NaOH 的质量分数为 6%～10%）浸泡 4 min，再在 30%HNO_3 溶液中浸泡 3 min，然后冲洗基材表面的残留溶液，烘干后放置于干燥箱内。焊前用丙酮溶液清洗基材表面。

图 1 为 2060 铝锂合金激光焦点旋转填丝焊接试验装置布置示意图。采用 YLS-6000 光纤激光器进行焊接试验，光束聚焦参数 K_f=8 mm·mrad，激光波长为 1060～1070 nm，传输光纤的芯径为 200 μm，准直镜焦距为 200 mm，聚焦镜焦距为 300 mm，聚焦光斑直径为 0.3 mm。采用前置送丝的方式进行焊接，焊接方向与母材轧制方向一致。焊接过程中采用氩气作为保护气体，氩气喷嘴轴线同母材法线的夹角为 45°，氩气流量为 15 L/min，焊缝背部采用氩气保护，氩气流量为 15 L/min。设计楔形镜的楔角，以获取所需激光聚焦点的旋转半径，通过激光焦点旋转装置控制楔形镜的转动速度。激光填丝焊和激光焦点旋转填丝焊的相关工艺参数如下：激光功率为 3.8 kW，焊接速度为 3 m/min，送丝角度（焊丝轴线同母材法线的夹角）为 45°，送丝速度为 3 m/min，光丝间距（激光旋转圆心与焊丝轴线在试样上接触位置的直线距离）为 0 mm。在试验过程中，采用 PHOTRON Fastcam 1024R2 彩色高速摄像仪观测焊接过程中的熔滴过渡行为。高速摄像时采用 808 μm 波段光源作为熔池的照明光。

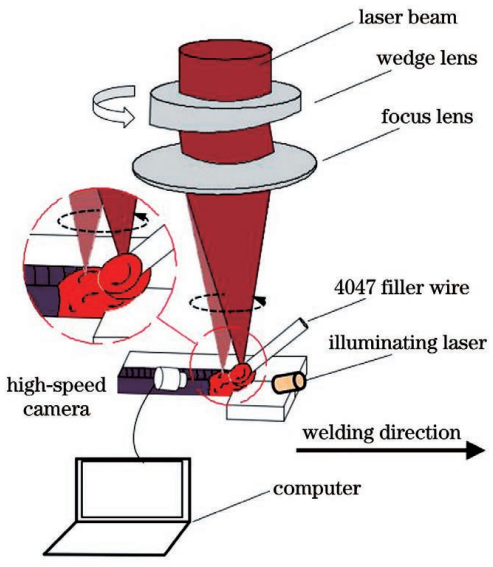

图 1 激光焦点旋转填丝焊接试验装置布置图

Fig. 1 Experimental setup for filler wire laser welding test with laser focus rotation

焊后制备金相试样，采用 Keller 试剂对其进行腐蚀，然后采用光学显微镜（OLYMPUS GX51）观察焊缝形貌及气孔缺陷。采用扫描电镜对接头进行显微组织观察并结合能谱仪（EDS）进行选区成分分析。采用 X 射线衍射仪（XRD）分析焊缝内不同区域的相组成。采用 FUTURE TECH-FM300e 型硬度仪对接头进行显微硬度测试，加载载荷为 0.98 N，加载时间为 15 s。

拉伸性能测试基于 ASTM 标准 E8m 进行，试样尺寸如图 2 所示。采用 CMT5305 拉伸试验机进行拉伸性能测试。

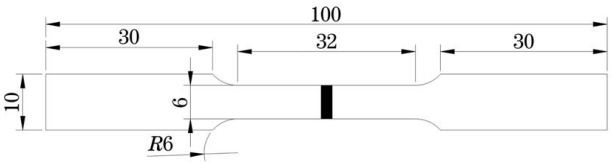

图 2 拉伸试样的形状与尺寸

Fig. 2 Shape and size of the test piece subjected to tensile test

3 试验结果与分析

3.1 焊缝形貌及气孔缺陷

激光焦点旋转半径和旋转频率对焊缝表面形貌及截面形貌的影响规律如表 1 所示。可见，采用激光焦点旋转填丝焊接工艺后，焊缝成形出现了明显变化，当旋转频率为 150 Hz 时，焊缝表面随旋转半径增加而更加光滑。与无旋转条件下相比，当旋转半径为 0.6～0.9 mm 时，正面焊缝整体更加饱满，无三角形鱼鳞纹形貌；当旋转半径大于 0.45 mm 时，焊缝周围飞溅数量明显减少，但当旋转半径为 0.9 mm 时，焊缝边缘出现了轻微的咬边现象。在激光填丝焊工艺中无论是否采用旋转工艺，焊缝横截面的成形均较为一致，均为中间存在束腰的 X 形，其中：当旋转半径大于等于 0.3 mm 时，焦点旋转填丝焊接头填充饱满，没有出现下塌现象；当旋转半径为 0.9 mm 时，焊缝中部束腰变宽，接头各位置的熔宽较为一致。

表 1　不同的激光焦点旋转半径 r 和旋转频率 f 下焊缝前表面及横截面的形貌

Table 1　Morphologies of weld front and cross-section under different focus rotation radii r and frequencies f

Radius of laser focus rotation	Morphologies of weld front and cross-section (f=150 Hz)	Laser focus rotation frequency	Morphologies of weld front and cross-section (r=0.6 mm)
No focus rotation	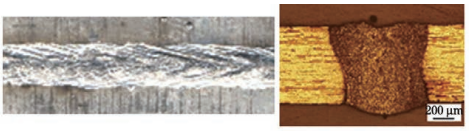	f=15 Hz	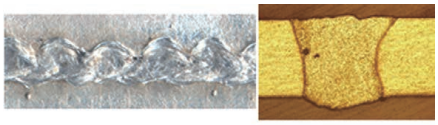
r=0.15 mm	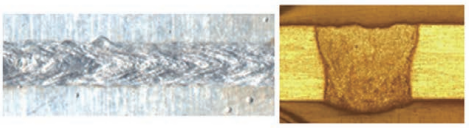	f=50 Hz	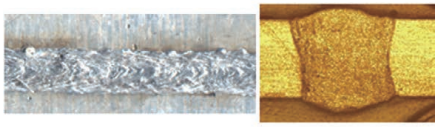
r=0.3 mm	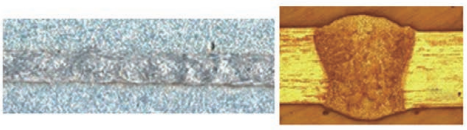	f=100 Hz	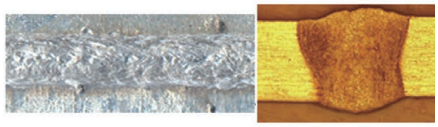
r=0.45 mm	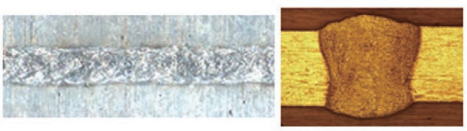	f=150 Hz	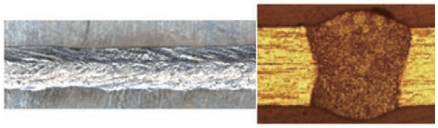
r=0.6 mm	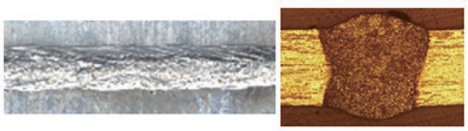	f=200 Hz	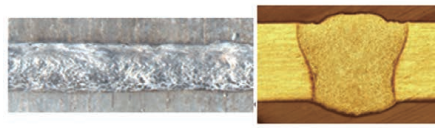
r=0.9 mm	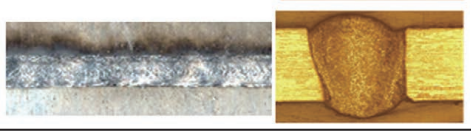	f=250 Hz	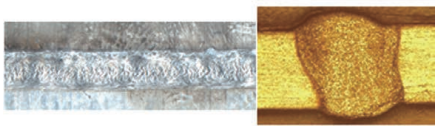

另外，在旋转半径为 0.6 mm 的条件下，当采用低旋转频率 15 Hz 焊接时，激光焦点运动路径导致焊缝呈麻花状，此时的焊缝成形质量较差，焊缝周边存在较多飞溅；当旋转频率提高至 50 Hz 后，麻花状消失，焊缝正面存在不规则的凸起、下塌，边缘存在未熔化的毛刺；当旋转频率提高至 100～200 Hz 之间时，焊缝正面光滑，鱼鳞纹变浅，焊缝边缘宽度较为一致，焊缝周围的飞溅得到了明显抑制；当旋转频率提高到 250 Hz 后，焊缝表面的鱼鳞纹基本消失，但焊缝起伏较大，填充均匀性不够理想，并且焊缝边缘出现了轻度咬边现象。

通过高速摄像图对比分析一个旋转周期内焦点旋转和非焦点旋转工艺下焊丝及母材的熔化行为，如图 3、4 所示。在激光焦点旋转填丝焊接过程中（旋转半径为 0.6 mm，频率为 150 Hz），激光焦点周期性地作用在熔池、焊丝末端，熔池波动幅度小，保持平稳，无飞溅产生；而在激光非旋转填丝焊接过程中，熔池波动较大，有飞溅产生（t+7.5 ms）。两者的焊丝过渡行为均为液桥过渡。由此可知，激光焦点旋转会改变熔池的流动行为，进而改变焊缝表面

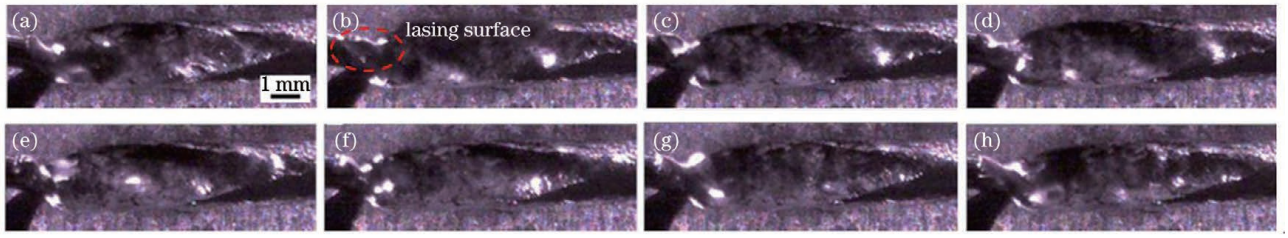

图 3　激光焦点旋转填丝焊的高速摄像图。(a) t+0 ms；(b) t+1 ms；(c) t+2 ms；(d) t+3 ms；(e) t+4 ms；(f) t+5 ms；(g) t+6 ms；(h) t+7 ms

Fig. 3　Images taken in filler wire laser welding with laser focus rotation by using a high-speed camera. (a) t+0 ms; (b) t+1 ms; (c) t+2 ms; (d) t+3 ms; (e) t+4 ms; (f) t+5 ms; (g) t+6 ms; (h) t+7 ms

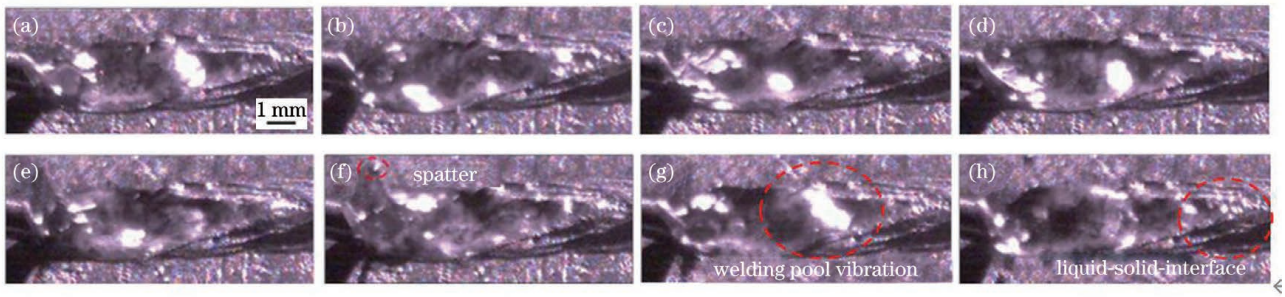

图 4　激光非旋转填丝焊的高速摄像图。(a) t+0 ms;(b) t+1.5 ms;(c) t+3 ms;(d) t+4.5 ms;(e) t+6 ms;(f) t+7.5 ms;(g) t+9 ms;(h) t+10.5 ms

Fig. 4　Images taken in filler wire laser welding without laser focus rotation by using a high-speed camera. (a) t+0 ms; (b) t+1.5 ms; (c) t+3 ms; (d) t+4.5 ms; (e) t+6 ms; (f) t+7.5 ms; (g) t+9 ms; (h) t+10.5 ms

形貌和飞溅行为。

根据本课题组的前期研究结果,在铝合金非填丝扫描焊接 8 mm 厚 1060 铝合金中,激光焦点高速旋转可以引导熔池的熔化和凝固行为,使焊缝表面的鱼鳞纹由非旋转时的三角形变为圆弧形[16]。但焦点旋转填丝焊缝表面没有出现圆弧形的鱼鳞纹,这是因为两者的焊接条件不同,从而导致焊缝熔池的形状不同。

此次试验为激光填丝穿透焊,熔池呈长圆形。熔池的形状既与激光功率等热输入条件有关,还与母材形状及材质有关。由于母材厚度为 2 mm,并且焊缝下部的支撑工装加工有氩气保护槽,所以与 8 mm 非穿透焊相比,母材的散热大大减少,熔化特性大大增强。另外,铝合金的熔点低,熔池表面张力小,填充焊丝的加入拓宽了熔池尺寸。因此,激光旋转在熔池中的扫描轨迹与熔池凝固的固液界面尚有一定距离,激光的周期性运动只能引起熔池流动,不会对熔池凝固处的固液界面产生引导作用。在本试验中,激光旋转对熔池流动的周期性振荡虽然不能使焊缝表面获得圆弧形鱼鳞纹形貌[16],但却改变了非旋转填丝焊接时的三角形鱼鳞纹形貌,优化了焊缝表面的成形。

如图 5 所示,两种焊接方式下获得的焊缝的横截面形貌基本相同,均呈现中间存在束腰的 X 形,焊缝上部、中部及下部的宽度变化不大。非旋转工艺接头内存在弥散分布及尺寸不一的气孔,而焦点旋转工艺接头只是在熔合线附近存在微小气孔,如图 5(d)所示(两种接头都有该类气孔)。通过高速摄像观察熔池流动和焊丝熔化过渡行为可知,在激光焦点旋转填丝焊接中,激光焦点高速旋转,导致激光周期性地作用在焊丝和熔池上,在一定程度上增加了熔池内部的对流,并增加了熔池的长度,这有利

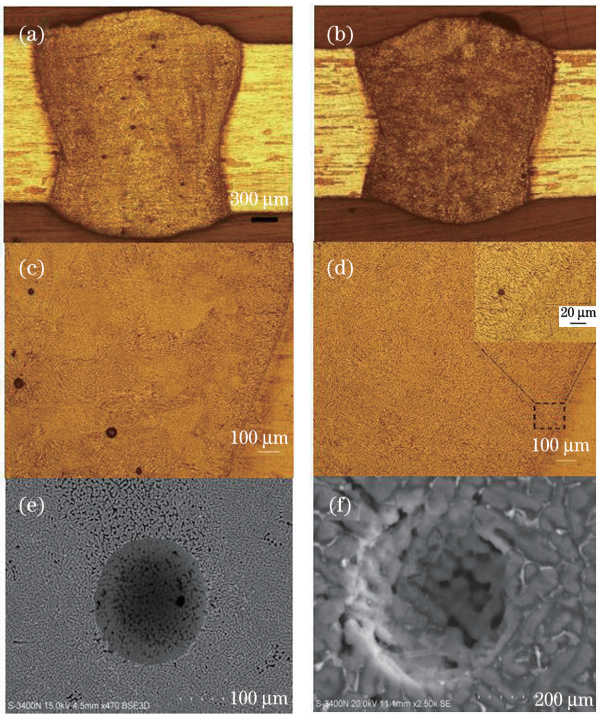

图 5　两种工艺下的焊缝形貌及气孔分布。(a)填丝焊焊缝横截面;(b)激光焦点旋转填丝焊焊缝横截面(f=150 Hz,r=0.6 mm);(c)激光焦点非旋转填丝焊接接头;(d)激光焦点旋转填丝焊接接头;(e)焊缝内尺寸较大的弥散气孔;(f)熔合线附近尺寸较小的气孔

Fig. 5　Weld morphologies and pore distributions under two welding processes. (a) Cross-section of the weld in filler wire laser welding; (b) cross-section of the weld in filler wire laser welding with focus rotation (f=150 Hz, r=0.6 mm); (c) welded joint in filler wire laser welding without focus rotation; (d) welded joint in filler wire laser welding with focus rotation; (e) dispersed pores of large sizes in the weld; (f) tiny pores around the fusion line

于气泡的上浮；另外，熔池的平稳流动也可以有效抑制保护气体卷入熔池，使接头中的气孔数量大幅减少，气孔尺寸大幅减小。

3.2　接头的微观组织分析

焦点旋转与不旋转焊接工艺下焊缝的显微组织如图 6 所示。可以看出，在激光非旋转填丝焊和激光焦点旋转填丝焊这两种焊接方式下，焊缝组织从熔合线附近到焊缝中心均依次为热影响区（HAZ 区）、部分熔融区（PMZ 区）、等轴细晶区（EQZ 区）、柱状晶区（CGZ 区）。

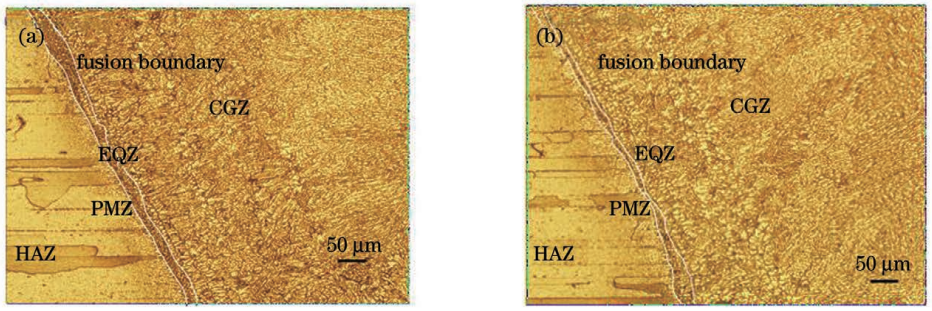

图 6　不同焊接工艺下接头熔合线附近的显微组织。(a)激光非旋转填丝焊；(b)激光焦点旋转填丝焊

Fig. 6　Microstructures of welded joint around the fusion lines under different welding processes. (a) Filler wire laser welding without focus rotation; (b) filler wire laser welding with focus rotation

为了进一步考察激光焦点旋转工艺对接头组织的影响，对接头各区域内的组织进行对比分析。图 7 和图 8 分别为两种焊接工艺下焊接接头各典型区域的组织形貌。

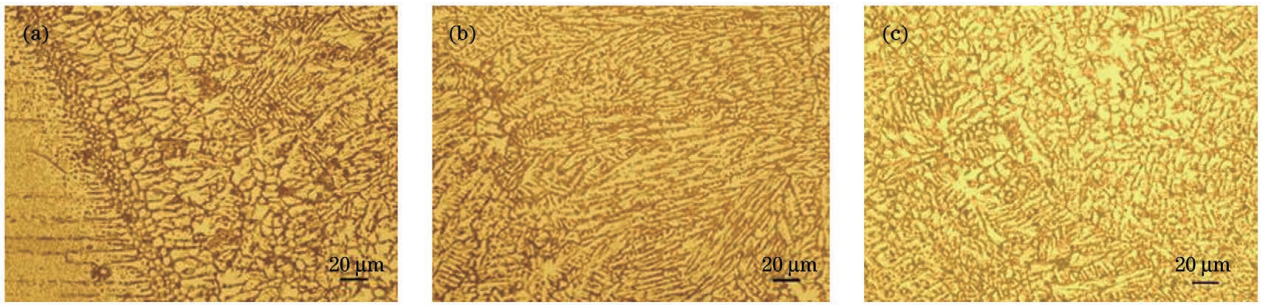

图 7　激光非旋转填丝焊接接头的显微组织。(a)熔合线附近；(b)熔合线至焊缝中心之间；(c)焊缝中心

Fig. 7　Microstructures of welded joint prepared by filler wire laser welding without focus rotation. (a) Near fusion line; (b) between fusion line and weld center; (c) weld center

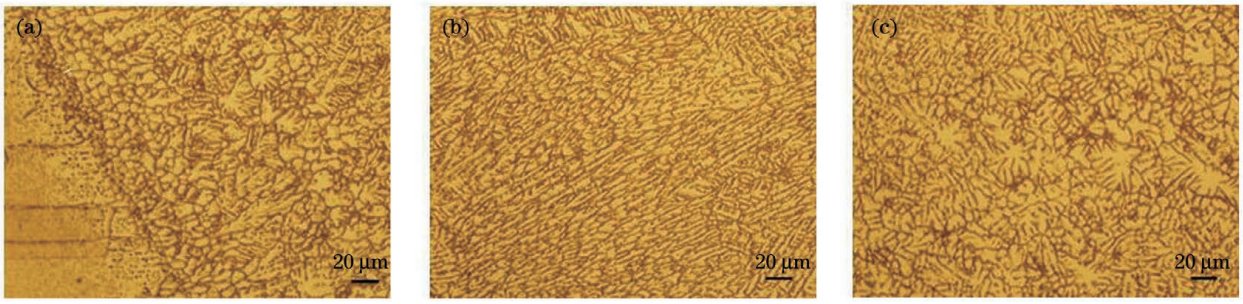

图 8　激光焦点旋转填丝焊接接头的显微组织。(a)熔合线附近；(b)熔合线至焊缝中心之间；(c)焊缝中心

Fig. 8　Microstructures of welded joint prepared by filler wire laser welding with focus rotation. (a) Near fusion line; (b) between fusion line and weld center; (c) weld center

对比图 7(a)和图 8(a)可以看出，采用焦点旋转工艺后，在熔合线附近的 PMZ 区仍可以观察到明显的粗大晶界，EQZ 区宽度范围有所缩小，并且靠近细晶区的柱状晶尺寸有所减小。激光焦点的旋转运动可能在一定程度上改变了熔池两侧（宽度方向）固液界面的温度梯度，对联生结晶过程产生影响，进而减小了柱状晶尺寸。

如图 7(b)和图 8(b)所示，在熔合线至焊缝中心之间的 CGZ 区，两种工艺的晶粒尺寸未见明显改变，说明焦点旋转对柱状晶的生长没有显著影响。

如图 7(c)和图 8(c)所示，采用焦点旋转工艺后，焊缝中心的晶粒尺寸略有增加，二次枝晶间距变小。这是因为激光焦点旋转行为导致局部重复加热[18]，增加了热输入，从而导致焊缝中心的等轴枝晶组织出现了一定程度的粗化。

3.3　焊缝内的元素分布

图 9 为激光非旋转填丝焊接与激光焦点旋转填丝焊接工艺下焊缝中心的背散射电子图像。可以看出，在两种焊接工艺下，焊缝中心均出现了元素在晶界和枝晶间富集的现象，但差别不大。

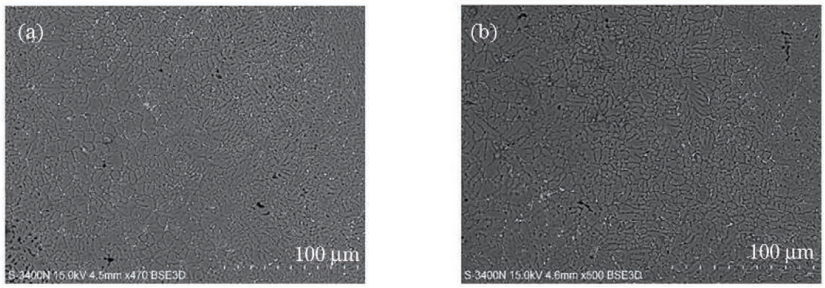

图 9　焊缝中心的背散射电子照片。(a)激光非旋转填丝焊；(b)激光焦点旋转填丝焊

Fig. 9　Back-scattered electron images of welds center. (a) Filler wire laser welding without focus rotation; (b) filler wire laser welding with focus rotation

图 10 为两种工艺下焊缝中心元素的面扫描结果。从图中可以看到，焊缝中心为等轴晶，并存在枝晶形貌。对比图 10(a)和图 10(b)可以发现，采用激光焦点旋转工艺后，晶粒尺寸较大，焊缝组织观察结果与金相显微镜的观察结果一致。从元素的面扫描结果来看，两种工艺下焊缝中心的合金元素分布不均匀，合金元素除了在 α(Al)基体内富集，还在枝晶间偏聚。微区成分分析结果显示，在枝晶间偏聚的元素主要是硅元素、铜元素以及少量镁元素，元素的分布情况差别不大。

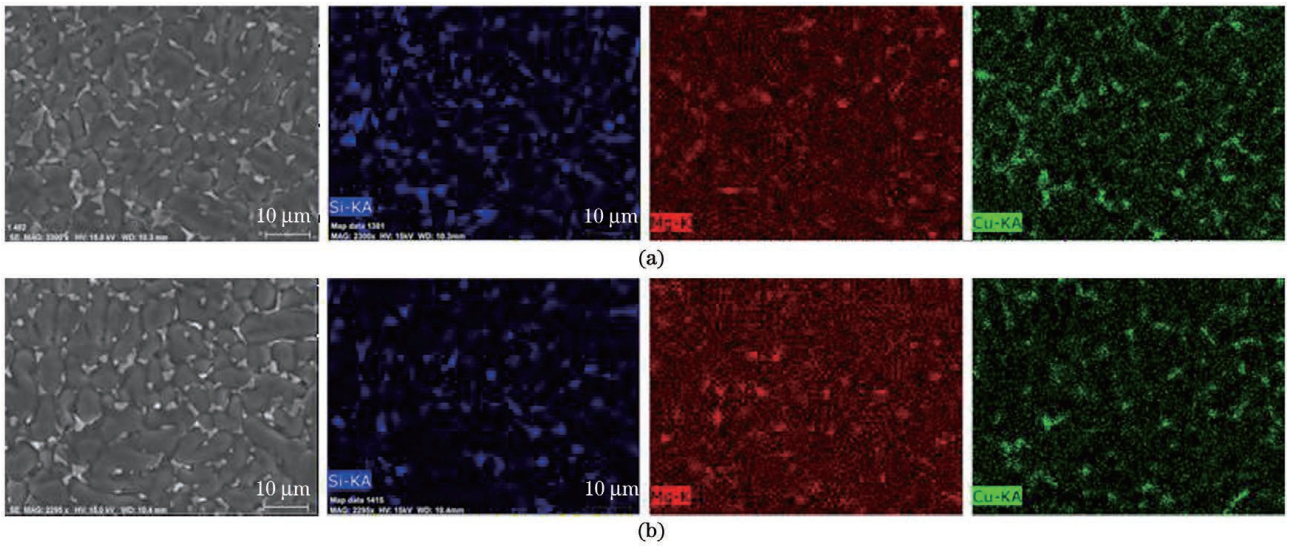

图 10　不同焊接工艺下焊缝中心元素的面分布。(a)激光非旋转填丝焊；(b)激光焦点旋转填丝焊

Fig. 10　Surface distributions of elements in central areas of welds prepared with two different welding processes. (a) Filler wire laser welding without focus rotation; (b) filler wire laser welding with focus rotation

图 11 为两种工艺下焊缝中心的二次电子图像，从图中可以观察到在枝晶间及晶界上存在多种形态及尺寸的析出相，且以三角形析出相和长条形析出相为主。旋转工艺对析出相的位置及形态等没有明显影响。

对焊缝进行 XRD 测试，XRD 图谱如图 12 所示。经过对比分析可知，旋转工艺的使用基本不会改变析出相的种类，两种工艺下的主要析出相均为 α(Al)固溶体、θ 相(Al_2Cu)和 T 相(AlLiSi)。

3.4　力学性能测试

图 13 为激光焦点旋转填丝焊和激光非旋转填丝焊接头横截面上的显微硬度分布。可以看出：在 PMZ 区，两者均出现了硬度低值，约为 95 HV0.1。在激光焊接过程中，熔合线附近母材的温度较高，导

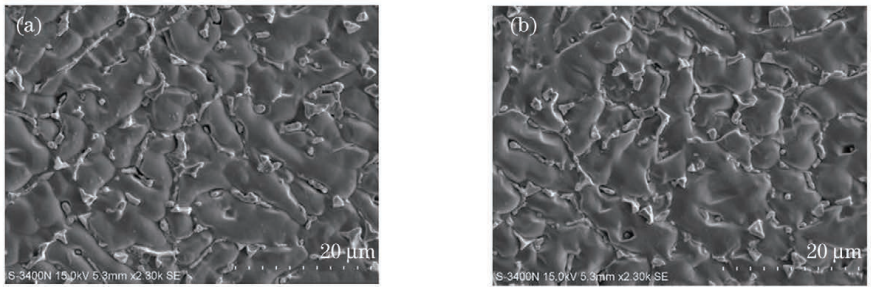

图 11　焊缝中心的二次电子图像。(a)激光非旋转填丝焊;(b)激光焦点旋转填丝焊

Fig. 11　Secondary electron images of welds center. (a) Filler wire laser welding without focus rotation; (b) filler wire laser welding with focus rotation

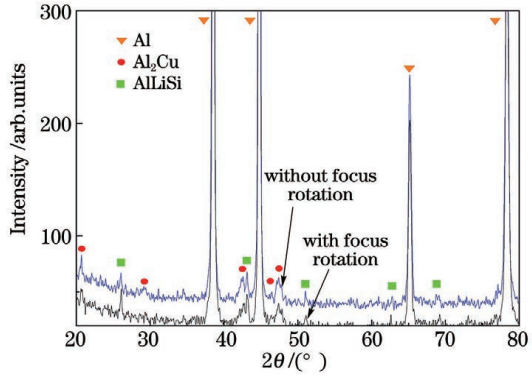

图 12　两种焊缝的 XRD 图谱

Fig. 12　XRD patterns of two welds

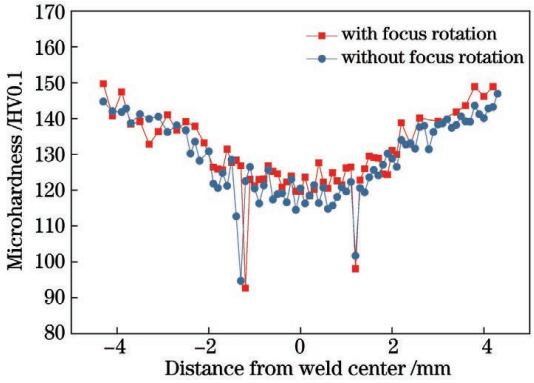

图 13　两种接头的显微硬度

Fig. 13　Microhardness of two welded joints

致过时效效应,母材中的强化相熔解,因此 PMZ 区的显微硬度显著降低。采用旋转焊接工艺后,PMZ 区的接头软化现象无明显改善。在激光非旋转工艺下,焊缝中心的硬度降到了母材的 76%,约为 115 HV0.1;在焦点旋转工艺下,整个接头的硬度更加均匀,约为 123 HV0.1,是母材的 82%,相较非旋转工艺下的接头显微硬度提高了 6.9%。

拉伸试验结果如图 14 所示。与激光焦点非旋转工艺下获得的焊缝接头的抗拉强度(349.4 MPa)相比,激光焦点旋转工艺下获得的接头的抗拉强度略高,为 365.0 MPa,两者差别很小。拉伸测试结束

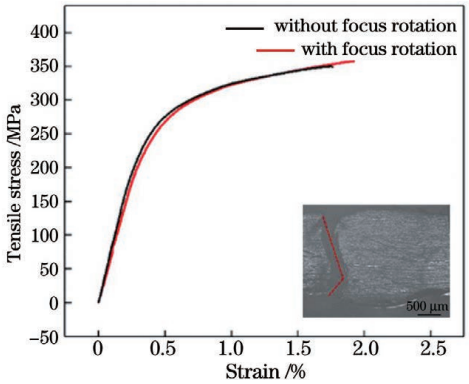

图 14　焊接试样的拉伸应力-应变曲线

Fig. 14　Tensile stress-strain curves of test pieces in two welding processes

后,焊接接头均在熔合线附近断裂,这是因为焊接接头在熔合线附近发生了明显的强度弱化。接头强度在一定程度上与接头的显微硬度相匹配,根据测试结果,PMZ 区出现了明显的硬度低值,说明熔合线附近区域出现了明显的接头弱化现象,该位置是接头拉伸测试时的薄弱位置。

对拉伸断口进行扫描电镜观察,观察结果如图 15 和图 16 所示。整体来看,两种拉伸断口均表现为韧窝聚集型沿晶断裂,具有混合断裂的特征。

两种焊接工艺下的焊缝上部与下部均存在较多微小韧窝,如图 15(a)、(c)与图 16(a)、(c)所示,韧窝尺寸及深浅无明显区别,断口中部均呈沿晶断裂形貌。非旋转焊接试样断口上存在较多气孔,断口上的气孔都为圆形。

4　结　　论

激光焦点的高频旋转使其周期性地作用在焊缝熔池及焊丝末端,同非焦点旋转填丝焊接相比,熔池长度有所增加,熔池流动更加平稳且波动幅度更小,有利于改善焊缝成形、抑制飞溅和减少气孔缺陷。

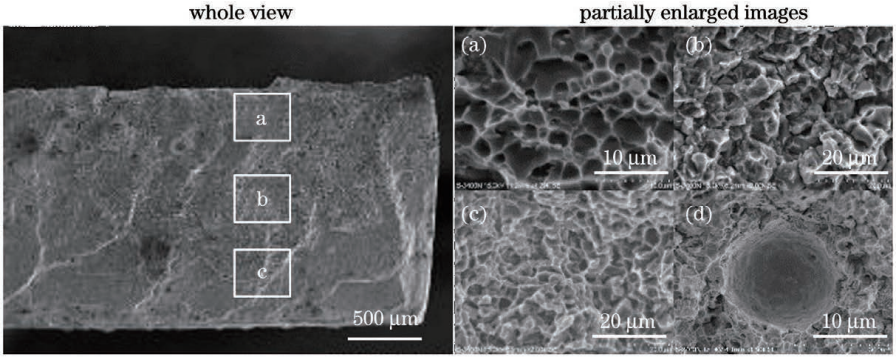

图 15 激光非旋转填丝焊试样拉伸断口的 SEM 图像。(a)区域 a;(b)区域 b;(c)区域 c;(d)气孔

Fig. 15 SEM images of tensile fracture of test pieces prepared by filler wire laser welding without focus rotation. (a) Area a; (b) area b; (c) area c; (d) pore

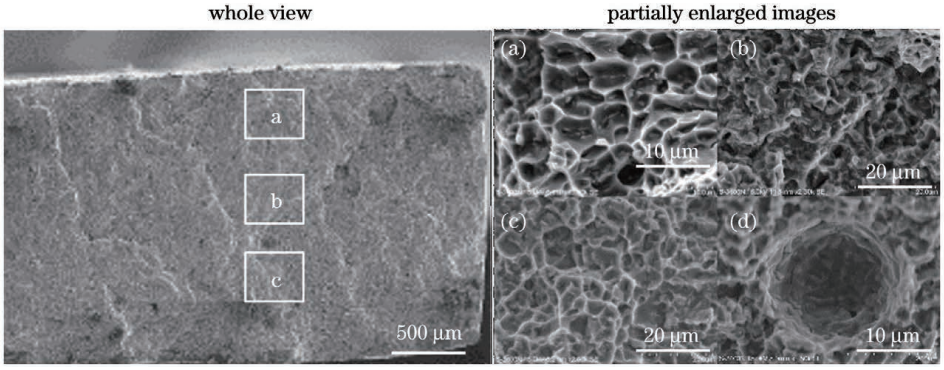

图 16 激光焦点旋转填丝焊试样拉伸断口的 SEM 图像。(a)区域 a;(b)区域 b;(c)区域 c;(d)气孔

Fig. 16 SEM images of tensile fracture of test pieces prepared by filler wire laser welding with focus rotation. (a) Area a; (b) area b; (c) area c; (d) pore

与激光焦点非旋转焊接工艺相比,激光焦点旋转填丝焊接工艺获得的接头中的 EQZ 区宽度、EQZ 区晶粒尺寸和靠近细晶区的柱状晶尺寸有所减小。

与激光焦点非旋转焊接接头相比,激光焦点旋转填丝焊接接头熔合线附近的显微硬度和拉伸强度略有升高,接头断裂在熔合线附近,拉伸断口呈混合断裂特征。

参 考 文 献

[1] Akhtar W, Akhtar N, Wu S J. Future of new generation aluminium and composites in aerospace industry[J]. Pakistan Journal of Chemistry, 2014, 4(2): 77-82.

[2] Xia L, Kang Y, Yu H S, et al. Equiaxed grains in laser welded 2060 Al-Li alloys and their formation mechanism[J]. Chinese Journal of Lasers, 2018, 45(11): 1102013.
夏令, 康悦, 余海松, 等. 2060 铝锂合金激光焊接等轴晶带及其形成机理[J]. 中国激光, 2018, 45(11): 1102013.

[3] Xiao R S, Zhang X Y. Problems and issues in laser beam welding of aluminum-lithium alloys[J]. Journal of Manufacturing Processes, 2014, 16(2): 166-175.

[4] Jia S H, Jia J P, Jiao J K, et al. Experimental and numerical studies on laser stir welding of carbon fiber reinforced thermal polymers/aluminum alloy [J]. Chinese Journal of Lasers, 2019, 46(7): 0702006.
贾少辉, 贾剑平, 焦俊科, 等. 碳纤维增强热塑性复合材料/铝合金激光搅拌焊接实验及仿真研究[J]. 中国激光, 2019, 46(7): 0702006.

[5] Zhao L, Cao Z, Zou J L, et al. Keyhole morphological characteristics in high-power deep penetration fiber laser welding[J]. Chinese Journal of Lasers, 2020, 47(11): 1102005.
赵乐, 曹政, 邹江林, 等. 高功率光纤激光深熔焊接小孔的形貌特征[J]. 中国激光, 2020, 47(11): 1102005.

[6] Chen K, Yang W X, Xiao R S. Direct laser welding for Al-Li alloy plate without prior surface cleaning [J]. Lasers in Engineer, 2012, 22: 361-369.

[7] Xiao R S, Yang W X, Chen K. Porosity characterization in laser welds of Al-Li alloy 1420[J]. Applied Laser, 2007, 27(1): 13-17.
肖荣诗, 杨武雄, 陈锴. 1420 铝锂合金激光焊接气孔行为特性研究[J]. 应用激光, 2007, 27(1): 13-17.

[8] Sun Z, Kuo M. Bridging the joint gap with wire feed laser welding[J]. Journal of Materials Processing Technology, 1999, 87(1/2/3): 213-222.

[9] Ram G D J, Mitra T K, Raju M K, et al. Use of inoculants to refine weld solidification structure and improve weldability in type 2090 Al-Li alloy[J]. Materials Science and Engineering A, 2000, 276(1/2): 48-57.

[10] Zhang X Y, Yang W X, Xiao R S. Microstructure and mechanical properties of laser beam welded Al-Li alloy 2060 with Al-Mg filler wire[J]. Materials & Design, 2015, 88: 446-450.

[11] Zhang X Y, Huang T, Yang W X, et al. Microstructure and mechanical properties of laser beam-welded AA2060 Al-Li alloy[J]. Journal of Materials Processing Technology, 2016, 237: 301-308.

[12] Yu Y C, Huang W, Wang G Z, et al. Investigation of melting dynamics of filler wire during wire feed laser welding[J]. Journal of Mechanical Science and Technology, 2013, 27(4): 1097-1108.

[13] Schultz V, Seefeld T, Vollertsen F. Gap bridging ability in laser beam welding of thin aluminum sheets [J]. Physics Procedia, 2014, 56: 545-553.

[14] Twardowska A, Kusinski J P. Laser welding of Al-Li-Mg-Zr alloy[J]. Proceedings of SPIE, 2000, 4238: 180-185.

[15] Hugger F, Hofmann K, Kohl S, et al. Spatter formation in laser beam welding using laser beam oscillation[J]. Welding in the World, 2015, 59(2): 165-172.

[16] Wang L, Gao M, Zhang C, et al. Effect of beam oscillating pattern on weld characterization of laser welding of AA6061-T6 aluminum alloy[J]. Materials & Design, 2016, 108: 707-717.

[17] Wu Q, Xiao R S, Zou J L, et al. Weld formation mechanism during fiber laser welding of aluminum alloys with focus rotation and vertical oscillation[J]. Journal of Manufacturing Processes, 2018, 36: 149-154.

[18] Peng S S, Zou J L, Li X T, et al. Fiber laser high-frequency focus rotation spot welding process based on thermal conductivity[J]. Chinese Journal of Lasers, 2018, 45(11): 1102011.
彭书胜, 邹江林, 李新桐, 等. 基于热导机制的光纤激光焦点高频旋转点焊工艺[J]. 中国激光, 2018, 45(11): 1102011.

Fiber Laser Filler Wire Welding of 2060 Aluminum-Lithium Alloy with Laser Focus Rotation

Wu Qiang*, Jiang Renjie, Li Xingtong, Zou Jiangling, Xiao Rongshi

Intelligent Photonic Manufacturing Center, Faculty of Materials and Manufacturing, Beijing University of Technology, Beijing 100124, *China*

Abstract

Objective 2060 aluminum-lithium alloy is a third-generation aluminum-lithium alloy, which has excellent performance, such as low density and high specific stiffness. It has broad application prospects in the aerospace field. Fiber laser welding technology is rapidly developing because of high welding speed and high efficiency. The lightweight material of the aluminum-lithium alloy, combined with fiber laser welding, can satisfy the lightweight requirements of aircraft. Because of the large thermal expansion coefficient of the aluminum-lithium alloy and easy burning of elements, the problems of cracks, pores, and mechanical properties are concerning. Although the crack-assisted process can effectively suppress cracks, the pores and mechanical properties still need to be improved. Moreover, the filler wire welding process causes problems such as high light wire matching and complicated melting and solidification behavior of the wire. In this study, focus rotation and filler wire were adopted in the fiber laser welding (denoted as laser welding-FRFW) of 2 mm-thick 2060 aluminum-lithium alloy to analyze the impact of laser focus rotation on the weld formation, porosity, distribution of microstructures in the weld, and the mechanical properties of the welded joint.

Methods The test specimen was a piece of 2060-T8 aluminum-lithium alloy. We used 4047 welding wires with a diameter of 1.2 mm. The YLS-6000 fiber laser was used. The core diameter of the transmission fiber was 200 μm, the focal length of the collimating lens was 200 mm, and the focal length of the focus lens was 300 mm. The wedge angle of the wedge prism was designed to obtain the required laser focus rotation radius. A laser focus rotating device

was used to regulate the rotational speed of the wedge prism. We adopted the process parameters as follows: laser power, 3.8 kW; welding speed, 3 m/min; wire-feeding angle, 45°; wire-feeding speed, 3 m/min; laser-wire distance, 0 mm. Furthermore, a color high-speed camera was used to observe the droplet transfer behavior in the welding process. When the welding was completed, we prepared metallographic specimens for analyzing the weld morphologies and porosity. Scanning electron microscopy was used to observe the microstructures of welded joints. A scanning electron microscope and an energy dispersive spectrometer (EDS) were used to analyze the ingredients of any selected area. Further, X-ray diffraction (XRD) was used to analyze phase compositions in different areas within the weld. We used a hardness tester to measure the microhardness of the welded joints with the load of 0.98 N loaded for 15 s. The tensile properties of welds were tested based on the ASTM E8m standard.

Results and Discussions The weld morphology considerably changed after applying laser welding-FRFW (Fig. 1). The surface of the weld was smooth with shallower fish scale-shaped ripples; the width of the entire weld became more uniform; and the spatters around the weld were effectively suppressed. The laser focus periodically acted on the weld pool and the end of the welding wire, and the weld pool was stable with a small fluctuation range and no spatter (Fig. 3 and Fig. 4), and there were only tiny pores around the fusion line (Fig. 5). The laser focus periodically acted on the welding wire and weld pool. This action can make the weld pool longer, making it easier for bubbles to move upwards and escape the weld pool.

There were four zones distributed from the fusion line to the center of the weld: HAZ, PMZ, EQZ, and CGZ (Fig. 6). When focus rotation was applied, the obvious thick grain boundary could still be observed in the PMZ near the fusion line. Further, the width of the EQZ was reduced, and the sizes of column grains near the equiaxed grain zone became smaller [Fig. 7(a) and Fig. 7(b)]. The main precipitated phases are α (Al) solid solution, θ phase (Al_2Cu), and T phase (AlLiSi).

The low hardness appeared in the PMZ in both cases(Fig. 13). In filter wire laser welding, the strength at the weld center was reduced to approximately 115 HV0.1. When focus rotation was applied, the strength of the entire welded became more uniform and increased to approximately 123 HV0.1. Compared with that of the filler wire laser welding without focus rotation, the microhardness of the welded joint prepared by filler wire laser welding with focus rotation was increased by 6.9%. According to the tensile test results (Fig. 14), the tensile strength of the welded joint of laser welding-FRFW was 365.0 MPa, which is slightly higher than 349.4 MPa (the joint of filter wire laser welding). Fracture of each welded joint occurred in the area near the fusion line of the welds. Fractures of the welded joints obtained in both welding processes were dimple-aggregation type intergranular fractures with features of mixed fractures.

Conclusions Because of the high-frequency rotation of the laser focus, the laser focus could act periodically on the weld pool and one end of the welding wire. Based on the laser welding-FRFW, the weld pool was longer and more stable, which can improve the weld morphology, suppress spatters and reduce the number of pores. The width of the EQZ and sizes of the grains in EQZ as well as the sizes of the columnar grains near the equiaxed grain zone on the weld were reduced in the laser welding-FRFW. The microhardness near the fusion line and tensile strength of the welded joint were slightly increased compared with the filter wire laser welding without focus rotation. Moreover, the fracture of the welded joint, with features of mixed fractures, occurred near the fusion line.

Key words laser technique; aluminum-lithium alloy; welding with filler wire; fiber laser; focus rotation; microstructure; mechanical properties

OCIS codes 140.3390; 160.3900; 350.3850